A general classification of three-dimensional flow fields

M. S. Chong, A. E. Perry, and B. J. Cantwell

Citation: Physics of Fluids A: Fluid Dynamics **2**, 765 (1990); doi: 10.1063/1.857730
View online: https://doi.org/10.1063/1.857730
View Table of Contents: https://aip.scitation.org/toc/pfa/2/5
Published by the American Institute of Physics

A general classification of three-dimensional flow fields

M. S. Chong and A. E. Perry
Department of Mechanical Engineering, University of Melbourne, Melbourne, Australia
B. J. Cantwell
Department of Aeronautics and Astronautics, Stanford University, Stanford, California 94305

(Received 11 November 1988; accepted 17 January 1990)

The geometry of solution trajectories for three first-order coupled linear differential equations can be related and classified using three matrix invariants. This provides a generalized approach to the classification of elementary three-dimensional flow patterns defined by instantaneous streamlines for flow at and away from no-slip boundaries for both compressible and incompressible flow. Although the attention of this paper is on the velocity field and its associated deformation tensor, the results are valid for any smooth three-dimensional vector field. For example, there may be situations where it is appropriate to work in terms of the vorticity field or pressure gradient field. In any case, it is expected that the results presented here will be of use in the interpretation of complex flow field data.

I. INTRODUCTION

Modern experimental and computational fluid mechanics is increasingly concerned with the three-dimensional nature of fluid motion. Rapid advances in computer science and experimental instrumentation have made it possible to generate vast quantities of data. Before similar advances can occur in our ability to grasp complex fluid motion there is a need for a systematic study of basic three-dimensional flow fields and their diagrammatic representation. Such a study is presented here in the hope that it will provide a framework for the interpretation of complex flow data in terms of elementary flow patterns. In the past the study of flow topology has been confined mainly to incompressible flow (Perry and Chong[1]). More recent work in the simulation of compressible flows (Kaynak *et al.*[2] and Chen, Cantwell, and Mansour[3]), and in the measurement of flows with heat release (Lewis *et al.*[4]), has revealed a larger variety of local flow fields than occurs in incompressible flow. These new motions need to be analyzed and classified.

In this paper we consider fluid motions that are describable by the leading terms of a Taylor series expansion for the velocity field in terms of space coordinates. This excludes such singular cases as vortex sheets and shock waves. The coordinate system is assumed to translate without rotation with the origin following a fluid particle. In such a reference frame the flow at the origin is a critical point and the coefficients of the linear terms are elements of the rate-of-deformation tensor. If the origin of the coordinate system is located at a no-slip boundary and if a critical point occurs at the origin, the expansion starts with second-order terms and the interpretation of the associated coefficients is more complicated. In unsteady flow, the expansion is applied at an instant in time and the solution trajectories are obtained by integrating the velocity field assuming that the field is frozen in time. This gives instantaneous streamlines as defined by Perry and Chong[1] and other workers in this field.

The work is concerned with the streamlines defined by the solution trajectories of three linear, coupled, first-order ordinary differential equations. Although the eigenvalues and eigenvectors of the associated 3×3 matrix can be determined with elementary, well-known techniques, the relationship between these properties of the matrix and the geometry of the solution trajectories is neither well known nor well understood despite the classical nature of the subject. For example, unknown to many researchers, some of the current arguments over the definition of a vortex are virtually discussions concerning the relative strengths of the rate-of-strain tensor and this is discussed in Sec. VI.

We have found that the relationship between the matrix properties and geometry is not trivial and that the topological classification of the geometry of the solution trajectories has never been fully elucidated. The problem is discussed briefly in the electrical engineering text by Blaquire,[5] and a classification of possible solution geometries is given in the paper of Reyn[6] who, in passing, discusses the possible usefulness of the approach in the interpretation of compressible flow patterns but does not directly connect his results with fluid mechanics. Moreover, neither author correctly described the properties of the three-dimensional space of matrix invariants that is used to relate eigenvalues and eigenvectors to the geometry of the solution trajectories. In the present work we have attempted to provide a complete description of all possible cases and to relate these to examples from fluid mechanics. In the process a number of new results have been obtained. We feel that the work will be of use in the interpretation of complex flow field data.

Historically, critical point theory has been used primarily to examine the solution trajectories of ordinary differential equations (e.g., see Kaplan,[7] Pontryagin,[8] Andronov *et al.*,[9] and Minorsky[10]). The technique can also be adopted to describe the topological features of flow patterns and is based on the idea mentioned earlier of forming a local Taylor series expansion of the flow field (see Perry and Fairlie[11] and Perry and Chong[1] for an extensive review of the method). A critical point is a point in the flow field where all three velocity components are zero and the streamline slope is indeterminate. In the past, the topologies of critical points in three-dimensional flows have been examined by the use of simple two-dimensional phase-plane methods. This approach

 0899-8213/90/050765-13$02.00

makes use of the fact that in three dimensions there are planes (which we will call the eigenvector planes) that contain solution trajectories. By considering each of the eigenvector planes in turn, the velocity field is expressed as a set of linearized Taylor series expansions which makes use of a 2×2 matrix. This has two invariants p and q and these invariants are used to define the various types of critical points (nodes, saddles, foci, and associated degenerate cases) that can be classified on a p-q chart (see Perry and Fairlie,[11] Perry and Chong,[1] and textbooks on ordinary differential equations such as those of Kaplan[7] and Hirsch and Smale[12]).

The eigenvector planes in many of the cases studied in the past were easily identified and located, particularly if there were planes of symmetry involved or if a solid surface was specified as a boundary to the pattern. In the more general case where such simplifying features are not present, it becomes necessary to use an analysis based on three invariants of a 3×3 Jacobian matrix to locate the eigenvector planes. These three invariants are sufficient to completely classify the topology of the three-dimensional flow pattern. Investigating the properties of the patterns in the various eigenvector planes is necessary only for determining the orientation of the critical point pattern (i.e., which plane contains the nodes, saddles, and/or foci).

II. THE TOPOLOGY OF THREE-DIMENSIONAL CRITICAL POINTS

A three-dimensional set of first-order differential equations can be written as

$$\begin{pmatrix}\dot{x}_1\\ \dot{x}_2\\ \dot{x}_3\end{pmatrix}=\begin{pmatrix}a_{11} & a_{12} & a_{13}\\ a_{21} & a_{22} & a_{23}\\ a_{31} & a_{32} & a_{33}\end{pmatrix}\begin{pmatrix}x_1\\ x_2\\ x_3\end{pmatrix} \tag{1}$$

or

$$\dot{\mathbf{x}}=\mathbf{A}\cdot\mathbf{x},$$

where a_{ij} are real constants. In the case of a fluid flow the a_{ij} are the elements of the rate-of-deformation tensor $\partial\dot{x}_i/\partial x_j$ evaluated at $(x_1,x_2,x_3)=(0,0,0)$. If the flow is steady then solution trajectories correspond to streamlines. If the flow is unsteady then solution trajectories correspond to particle paths, which, in general, do not coincide with streamlines except at an instant. This paper is limited to an identification of the various kinds of local streamline patterns that can occur in three-dimensional flows which can be locally linearized in space, and so, degenerate cases are excluded. Issues of structural stability, bifurcation processes, and the possible onset of chaos which arise when the topology of a general flow is considered, while of considerable importance, are not of primary concern here. (For a discussion of these aspects of the problem the reader is referred to the books by Hirsch and Smale,[12] Guckenheimer and Holmes,[13] and the recent text by Wiggins.[14])

Let the rate-of-deformation tensor be broken up into a symmetric and antisymmetric part $\partial\dot{x}_i/\partial x_j=S_{ij}+R_{ij}$, where $S_{ij}=(\partial\dot{x}_i/dx_j+\partial\dot{x}_j/\partial x_i)/2$ and $R_{ij}=(\partial\dot{x}_i/\partial x_j-\partial\dot{x}_j/\partial x_i)/2$ (not to be confused with the scalar invariant R defined later) are the rate-of-strain and rotation (or spin) tensors, respectively. If λ_1, λ_2, and λ_3 are the eigenvalues of $\mathbf{A}$, then

$$[\mathbf{A}-\lambda I]\mathbf{e}=0, \tag{2}$$

where $\mathbf{e}$ is the eigenvector. The eigenvalues can be determined by solving the characteristic equation

$$\det[\mathbf{A}-\lambda I]=0, \tag{3}$$

which, for a 3×3 matrix, can be written as

$$\lambda^3+P\lambda^2+Q\lambda+R=0, \tag{4}$$

where

$$P=-(a_{11}+a_{22}+a_{33})=-\mathrm{tr}[\mathbf{A}]=-S_{ii}, \tag{5}$$

$$Q=\begin{vmatrix}a_{11} & a_{12}\\ a_{21} & a_{22}\end{vmatrix}+\begin{vmatrix}a_{11} & a_{13}\\ a_{31} & a_{33}\end{vmatrix}+\begin{vmatrix}a_{22} & a_{23}\\ a_{32} & a_{33}\end{vmatrix}$$
$$=\tfrac{1}{2}(P^2-\mathrm{tr}[\mathbf{A}^2])=\tfrac{1}{2}(P^2-S_{ij}S_{ji}-R_{ij}R_{ji}), \tag{6}$$

and

$$R=-\begin{vmatrix}a_{11} & a_{12} & a_{13}\\ a_{21} & a_{22} & a_{23}\\ a_{31} & a_{32} & a_{33}\end{vmatrix}=-\det[\mathbf{A}] \tag{7}$$
$$=\tfrac{1}{3}(-P^3+3PQ-\mathrm{tr}[\mathbf{A}^3])$$
$$=\tfrac{1}{3}(-P^3+3PQ-S_{ij}S_{jk}S_{ki}-3R_{ij}R_{jk}S_{ki}).$$

The characteristic equation can have (i) all real roots which are distinct, (ii) all real roots where at least two roots are equal, or (iii) one real root and a conjugate pair of complex roots.

It can be shown that in the P-Q-R space the surface S_1, which divides the real solutions from the complex solutions, is given by

$$27R^2+(4P^3-18PQ)R+(4Q^3-P^2Q^2)=0, \tag{8}$$

where terms have been gathered to form a quadratic equation in R. Figure 1 shows the intersection of this surface with planes of constant P. On this surface, the eigenvalues are real but two of them are equal. It can be shown that for real P, Q, and R this surface can be split up into two surfaces, S_{1a} and S_{1b}, which are, respectively, given by

$$\tfrac{1}{3}P(Q-\tfrac{2}{9}P^2)-\tfrac{2}{27}(-3Q+P^2)^{3/2}-R=0 \tag{9}$$

and

$$\tfrac{1}{3}P(Q-\tfrac{2}{9}P^2)+\tfrac{2}{27}(-3Q+P^2)^{3/2}-R=0. \tag{10}$$

Note that S_1 is antisymmetric with respect to P.

Surface S_{1a} osculates (or kisses) surface S_{1b} to form a cusp. At the cusp the eigenvalues are real and all of them are equal.

The matrix $\mathbf{A}$ can be transformed to another matrix $\mathbf{A}'$, which is in canonical form, and matrices $\mathbf{A}$ and $\mathbf{A}'$ have the same eigenvalues. If the eigenvalues are real and distinct, $\mathbf{A}'$ is given by

$$\mathbf{A}'=\begin{pmatrix}\lambda_1 & 0 & 0\\ 0 & \lambda_2 & 0\\ 0 & 0 & \lambda_3\end{pmatrix}. \tag{11}$$

If the eigenvalues are complex $\mathbf{A}'$ is given by

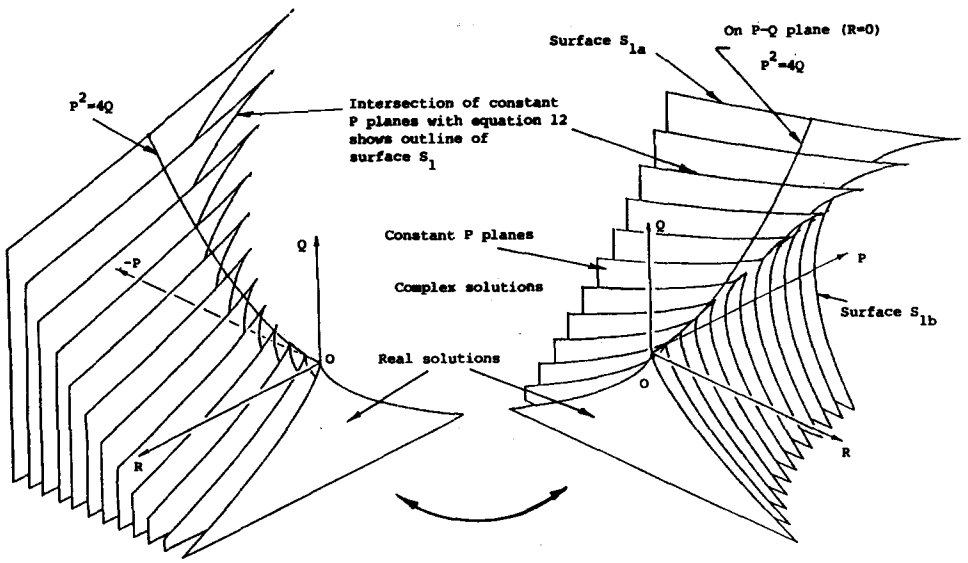

FIG. 1. The *P-Q-R* space showing surface S_1, which divides real solutions from complex solutions.

$$\mathbf{A}' = \begin{pmatrix} \sigma & -\omega & 0 \\ \omega & \sigma & 0 \\ 0 & 0 & b \end{pmatrix}, \tag{12}$$

where

$$\lambda_{1,2} = \sigma \pm i\omega,$$

$$\lambda_3 = b.$$

The solution in canonical form is

$$\dot{\mathbf{x}}' = \mathbf{A}' \cdot \mathbf{x}',$$

where

$$\mathbf{x}' = \mathbf{B} \cdot \mathbf{x}.$$

Here, **B** is the transforming matrix and from the above with Eq. (1) it can be shown that

$$\mathbf{B} \cdot \mathbf{A} = \mathbf{A}' \cdot \mathbf{B} \tag{13}$$

or

$$\dot{\mathbf{x}}' = (\mathbf{B} \cdot \mathbf{A} \cdot \mathbf{B}^{-1}) \cdot \mathbf{x}'. \tag{14}$$

Since it is always possible to find a matrix **B** that transforms the noncanonical solutions to the canonical solutions, it would be more convenient to consider the solution trajectories in canonical form where, if the eigenvalues are real,

$$P = -(\lambda_1 + \lambda_2 + \lambda_3), \tag{15}$$

$$Q = \lambda_1\lambda_2 + \lambda_1\lambda_3 + \lambda_2\lambda_3, \tag{16}$$

$$R = -\lambda_1\lambda_2\lambda_3, \tag{17}$$

and if the eigenvalues are complex,

$$P = -(2\sigma + b), \tag{18}$$

$$Q = \sigma^2 + \omega^2 + 2\sigma b, \tag{19}$$

$$R = -b(\sigma^2 + \omega^2). \tag{20}$$

Therefore, if P is fixed, solutions with real and different eigenvalues must lie in the shaded region shown in Fig. 2. This region is defined by

$$Q < P^2/3$$

and

$$R_a < R < R_b, \tag{21}$$

where

$$R_a = \tfrac{1}{3}P(Q - \tfrac{2}{9}P^2) - \tfrac{2}{27}(-3Q + P^2)^{3/2} \tag{22}$$

and

$$R_b = \tfrac{1}{3}P(Q - \tfrac{2}{9}P^2) + \tfrac{2}{27}(-3Q + P^2)^{3/2}. \tag{23}$$

If all the eigenvalues are real and if two of them are equal, then

$$R = R_a \quad \text{or} \quad R = R_b \tag{24}$$

and

$$Q < P^2/3.$$

If all the eigenvalues are real and equal, then

$$R = P^3/27, \quad Q = P^2/3. \tag{25}$$

If

$$Q > P^2/3,$$

we have one real root and a pair of complex conjugate roots, but if

$$Q < P^2/3,$$

we have one real root and a pair of complex conjugate roots when

$$R < R_a \quad \text{or} \quad R > R_b. \tag{26}$$

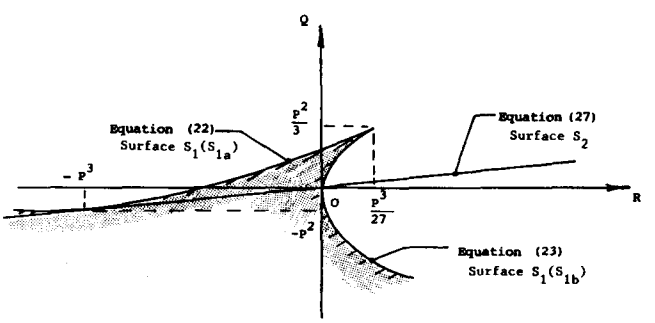

FIG. 2. The *Q-R* plane (P = const) showing the surface which divides the region of real solutions (shaded) from the region of complex solutions (unshaded).

If the complex eigenvalues are such that they are purely imaginary, it can be shown that they must lie on a surface S_2 given by

$$PQ - R = 0. \tag{27}$$

It can be shown that for constant P the surface S_2 intersects surface S_1 at $Q = 0, R = 0$, (i.e., along the P axis), and osculates the surface S_1 at $Q = -P^2$ and $R = -P^3$. The intersection and osculation merge to a point at the origin for $P = 0$ and S_2 contains the Q axis.

III. SOLUTION TRAJECTORIES

The possible combinations of solution trajectories in the various eigenvector planes are given in the following subsections.

A. Real solutions

If the eigenvalues are real and distinct there exist three eigenvector planes, defined by the linearly independent eigenvectors, which contain solution trajectories. All other solution trajectories asymptote to these eigenvector planes as the critical point is approached with the direction of time chosen appropriately. These eigenvector planes may contain nodes and saddles and the possible saddle–node combinations (readers are referred to Perry and Chong[1] for the definition of the various types of patterns) are nodes in all three eigenvector planes or saddles in two of the eigenvector planes and a node in the remaining eigenvector plane. A case of interest is when $R = 0$, which represents a two-dimensional pattern for the canonical case as shown in Fig. 3(a), and this two-dimensionality is skewed for the noncanonical case as shown in Fig. 3(b). This skewed two-dimensional flow or "planar" flow is also found to occur as a degenerate case in the three-dimensional separation pattern as studied by Perry and Fairlie[11] [see their Figs. 4(b) and 5(b)].

If the eigenvalues are real and two of them are equal (i.e., if we are on the surface S_{1a} or S_{1b} defined in Sec. II), then instead of having a node in one of the eigenvector planes we have a star node. In canonical form the matrix $\mathbf{A}'$ can be expressed as

$$\mathbf{A}' = \begin{pmatrix} \lambda_1 & 0 & 0 \\ 0 & \lambda & 0 \\ 0 & 0 & \lambda \end{pmatrix}. \tag{28}$$

In this case one coordinate plane will contain a star node. The direction of the eigenvector in this plane is indeterminate and any ray of the star node can be an "eigenvector." Hence any plane that is normal to the plane of the star node and passes through the origin will contain solution trajectories. However, it is not always possible to find a transformation that will diagonalize $\mathbf{A}$ into the canonical form given above. In such a case the canonical form must be expressed as

$$\mathbf{A}' = \begin{pmatrix} \lambda_1 & 0 & 0 \\ 0 & \lambda & 1 \\ 0 & 0 & \lambda \end{pmatrix}. \tag{29}$$

Here the solution trajectories in one of the coordinate planes form a degenerate logarithmic node where the solution trajectories are given by

$$x_2' = (1/\lambda)x_3' [\ln(Cx_3')]. \tag{30}$$

In this plane of the degenerate node there is only one eigenvector and there is only one other plane which will contain solution trajectories.

In this case where all the eigenvalues are real and equal (and this occurs at the point where surface S_{1a} osculates the surface S_{1b}), the forms of canonical solutions are given by

$$\mathbf{A}' = \begin{pmatrix} \lambda & 0 & 0 \\ 0 & \lambda & 0 \\ 0 & 0 & \lambda \end{pmatrix} \quad \text{or} \quad \mathbf{A}' = \begin{pmatrix} \lambda & 0 & 0 \\ 0 & \lambda & 1 \\ 0 & 0 & \lambda \end{pmatrix}$$

or

$$\mathbf{A}' = \begin{pmatrix} \lambda & 1 & 0 \\ 0 & \lambda & 1 \\ 0 & 0 & \lambda \end{pmatrix}. \tag{31}$$

In the first case we have star nodes everywhere (i.e., any plane that passes through the origin will contain solution trajectories). In the second case only two planes will contain solution trajectories. These will be the coordinate planes where one will contain a degenerate logarithmic node and the other will contain a star node. In the third case there will exist only one coordinate plane which contains solution trajectories and here we have a logarithmic node.

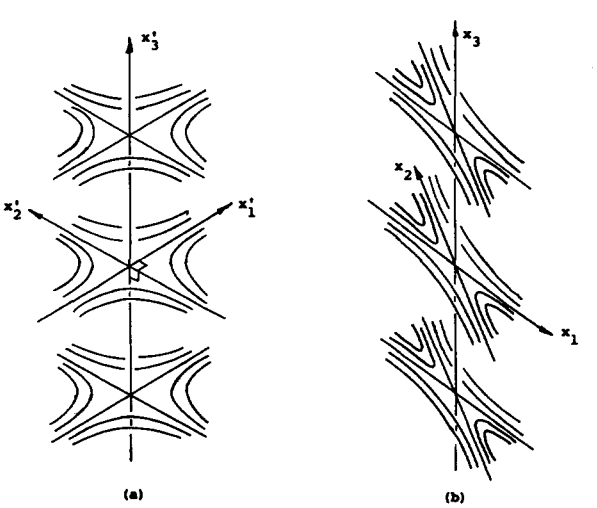

FIG. 3. Comparison between the two-dimensional critical point (canonical) and skewed two-dimensional critical point (noncanonical); (a) two-dimensional critical point; (b) skewed two-dimensional critical point.

B. Complex solutions

In canonical form the complex solutions are represented by Eqs. (18)–(20). There will exist only one plane that contains solution trajectories and in this plane we can have a focus or a center. Using polar coordinates it can be shown that in canonical form the solution trajectories are given by

$$r = Ce^{m\theta}, \tag{32}$$

where $m = \sigma/\omega$ and C depends on initial conditions.

From Eqs. (12) and (32), it can be seen that the topology of the flow pattern depends on m and b. It can be shown that

$$R = (P + 2\sigma)Q + 2\sigma(P + 2\sigma)^2. \tag{33}$$

Hence on a Q-R plane (i.e., a plane of constant P) lines of constant σ (and hence constant b) are straight lines and these lines osculate surface S_1 as shown in Fig. 4. In canonical form the sign of b determines whether the trajectory arrow is directed away or toward the plane that contains solution trajectories (i.e., the plane of the focus). In the case where b is positive, the spiraling is away from the plane of the focus [e.g., see Fig. 8(c) in the Appendix], and if b is negative the spiraling is toward the focus plane. The degenerate case is for $b = 0$ and here we have the two-dimensional case.

The rate and direction of spiral of the solution trajectories in the focus plane depend on m. For m positive we have an unstable focus (spiraling is away from the origin for increasing time) and for m negative we have a stable focus (spiraling is toward the origin for increasing time). The degenerate case is for $m = 0$ where instead of a focus we have a center. This corresponds to the case when $R = PQ$ [i.e., Eq. (27), surface S_2]. Hence this surface divides the complex zone into a region where the focus is stable and a region where the focus is unstable. For m approaching large values the rate of spiral of the solution trajectories will decrease and in the limit we obtain a star node. Also shown in Fig. 4 are lines of constant σ/ω.

A complete classification of all possible critical points has been carried out and is included in the Appendix.

IV. FREE-SLIP AND NO-SLIP CRITICAL POINTS

The critical point described by Eq. (1) is known as a free-slip critical point so as to distinguish from a second type of critical point that occurs on a no-slip boundary. If x_3 is the normal distance from the no-slip boundary, then by using a transformed time variable $d\tau = x_3\,dt$ and putting $\dot{x}_i = dx_i/d\tau$, Eq. (1) can be used for describing and classifying no-slip critical points (see Oswatitsch,[15] Lighthill,[16] and Perry and Fairlie[11]). However, the elements of matrix **A** will no longer be elements of the rate-of-deformation tensor but are higher-order quantities related to gradients of vorticity and pressure gradients. For details, the reader is referred to Perry and Fairlie[11] and Perry and Chong.[1] In the limit of $x_3 \to 0$ we have the so-called limiting surface streamlines, surface trajectories, or lines of surface shear stress.

The continuity equation for compressible flow is

$$\text{Div}\,\dot{\mathbf{x}} = -\frac{1}{\rho}\frac{D\rho}{Dt} = -\frac{1}{\rho}\left(\frac{\partial\rho}{\partial t} + \dot{x}_1\frac{\partial\rho}{\partial x_1} + \dot{x}_2\frac{\partial\rho}{\partial x_2} + \dot{x}_3\frac{\partial\rho}{\partial x_3}\right), \tag{34}$$

where $\dot{\mathbf{x}}$ is differentiated with respect to conventional time t. At a critical point, $\dot{x}_1 = \dot{x}_2 = \dot{x}_3 = 0$ and the flow divergence at the critical point is proportional to the time rate of change of the density at the point. If the flow is compressible and unsteady then it may be possible to obtain all the flow patterns described in Figs. 8(a)–8(f) in the Appendix. However, if the flow is incompressible or if the flow is compressible and steady then $\text{Div}\,\mathbf{x} = 0$ at the critical point and the number of possible flow patterns is limited. In this case

$$\frac{\partial\dot{x}_1}{\partial x_1} + \frac{\partial\dot{x}_2}{\partial x_2} + \frac{\partial\dot{x}_3}{\partial x_3} = a_{11} + a_{22} + a_{33} = 0. \tag{35}$$

A comparison of Eq. (35) with Eq. (5) shows that P must equal zero for this case. Therefore in the P-Q-R space all (steady or unsteady) incompressible or steady compressible free-slip critical points must lie on the plane $P = 0$. The types of possible flow patterns are shown in Fig. 8(b) in the Appendix.

Applying continuity to the no-slip critical points gives

$$a_{33} = -(a_{11} + a_{22})/2, \qquad a_{31} = a_{32} = 0, \tag{36}$$

for incompressible flow and steady imcompressible flow, and it can be shown that these critical points must lie on the surface S_3 defined by

$$PQ + 2P^3 + R = 0. \tag{37}$$

It can be shown that if the solution is complex the above equation still applies. Figure 5(a) shows surface S_3 in relation to surface S_1 and S_2 in a Q-R plane ($P = \text{const}$). It can be shown that S_3 intersects S_1 at $Q = -P^2$ and $R = -P^3$ (i.e., the point where S_2 osculates S_1). Surface S_3 also osculates S_1 at $Q = -5P^2$ and $R = 3P^3$. Figure 5(b) shows surfaces S_1, S_2, and S_3 in the Q-P plane ($R = \text{const}$).

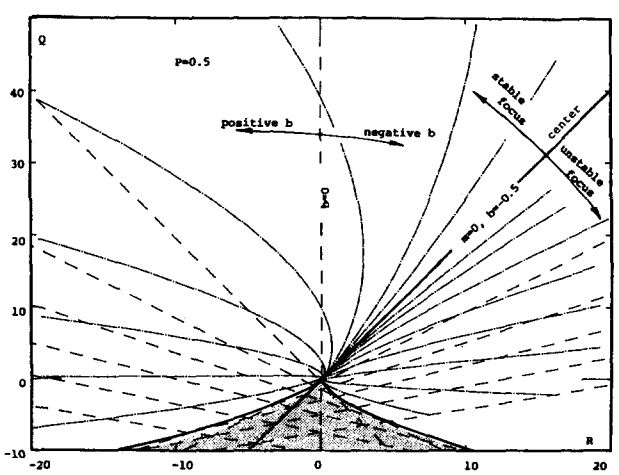

FIG. 4. Map of complex solutions. The complex region is shown unshaded; –·–: lines of constant $m = \sigma/\omega$; - - -: lines of constant b.

V. APPLICATION TO A THREE-DIMENSIONAL FLOW PATTERN

It is often difficult to study the topology of three-dimensional flow patterns, but with the use of the above classification the topology of the flow can be more easily understood. For example, Fig. 6 shows a three-dimensional separation pattern that has been classified as a U separation (Perry and Hornung[17]). The flow field has been obtained by solving the Navier–Stokes equations locally (see Perry and Chong[18]) using a third-order Taylor series expansion, and assuming that the flow pattern is symmetrical (i.e., $\dot{x}_1$ and $\dot{x}_3$ are assumed to be even in x_2 and $\dot{x}_2$ is assumed to be odd in x_2). The x_1-x_2 plane represents the no-slip boundary and this plane contains solution trajectories. Figure 6(a) shows the limiting surface streamlines on this plane. Because of the symmetry condition ($\dot{x}_2 = 0$ when $x_2 = 0$), the plane of symmetry (i.e., the x_1-x_3 plane) also contains solution trajectories and

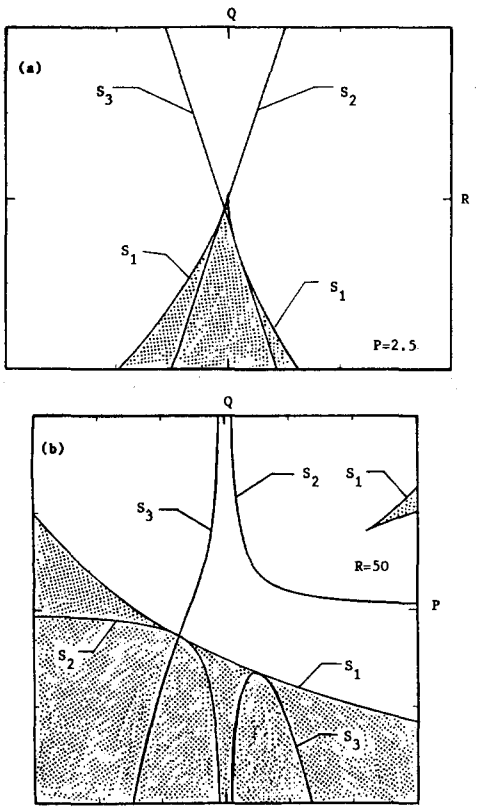

FIG. 5. Relation of surface S_3 to surfaces S_1 and S_2. No-slip critical points must lie on surface S_3. (a) Surfaces S_1, S_2, and S_3 for constant P. (b) Surfaces S_1, S_2, and S_3 for constant R.

Fig. 6(b) shows the solution trajectories in both the surface and the plane of symmetry. Hence it can be seen that there are three major critical points of interest [labeled 1, 2, and 3 in Fig. 6(b)]. Critical point 1 is a no-slip saddle and critical point 2 is a no-slip node in the x_1-x_2 plane. Critical point 3 is a free-slip focus in the x_1-x_3 plane.

The above flow pattern is an idealized one since perfectly symmetrical flow situations rarely, if ever, exist in practice. If the above flow pattern is perturbed slightly such that the symmetry condition is destroyed the geometry of the flow pattern is more difficult to "visualize." Figure 7(a) shows the surface streamline pattern for an unsymmetrical U separation. It can be seen that this is still topologically equivalent to the symmetrical pattern. However, the plane of symmetry is now destroyed and the no-slip surface is the only plane surface that contains solution trajectories for arbitrary distances from the origin. Figures 7(b) and 7(c) show an oblique view and side view, respectively, of the flow pattern and it can be seen that the trajectories above the surface are complicated. However, if we linearize the solution about the critical point above the surface and plot the linearized solution we can see from Fig. 7(d) that we have a free-slip focus above the surface and that the unsymmetrical U separation is topologically similar to the symmetrical U separation. Figure 7(e) shows the critical point above the surface such that the plane containing the focus is viewed "edge-on" and it can be seen that the focus is in a noncanonical form.

VI. WHEN IS A REGION OF VORTICITY A "VORTEX"?

There is currently occurring among many prominent workers in wall turbulence a debate as to how a vortex should be defined (see Lugt[19] and Kline[20]). Now that full direct simulations of the Navier–Stokes equations have recently been applied to wall turbulence (e.g., Spalart[21] and Robinson, Kline, and Spalart[22]), reliable computer-generated data are available which will enable a "picture" of the structure of wall turbulence to be constructed. Graphical representations of the velocity vector field and vortex lines have been constructed and the question many researchers are asking is whether there exist "horseshoe" vortices and whether the wall streaks are the result of longitudinal vortices in or near the sublayer region. Considerable confusion occurs when the instantaneous velocity vector fields are being discussed. The following are examples of statements that have been made regarding vortices.

"One must be careful when talking about vortices. There might be vorticity present but that does not necessarily mean that we have a vortex."

"Streamwise vortex lines persist for long streamwise distances but the streamwise vortices are quite short."

"A study of vortex lines suggests the existence of horseshoe vortices in wall turbulence but after examining the velocity vector field of some of these structures, one must conclude that only one leg is really a vortex."

These statements reflect typical conflicts which arise in the attempt to relate the instantaneous velocity and vorticity fields to the results of flow visualization, which usually involves the time-integrated effect of the flow on a tracer.

Hidden behind such statements are some implied vague unstated assumptions as to how a "vortex" should be defined. The instantaneous streamlines produced by integrating the velocity vector field resolved onto some chosen plane must exhibit either closed orbits or spirals. Also there is usually the notion of vortex lines being bunched or *vorticity* being concentrated. These qualities are usually thought to be essential aspects of a vortex. However, there are some difficulties. The topologies of velocity fields (and streamline patterns) depend on the velocity of the observer. Moreover, integrated particle paths can cross instantaneous streamlines in complicated ways. It has been shown by Cantwell and Allen[23] that a focus is produced in a low Reynolds number impulsively started jet without any local concentration of vorticity. It is our opinion that it is unlikely that any definition of a vortex will win universal acceptance. However, we suggest that a definition which might be acceptable to most is that a vortex core is a region of space where the vorticity is sufficiently strong to cause the rate-of-strain tensor to be dominated by the rotation tensor, i.e., the rate-of-deformation tensor has complex eigenvalues. This definition is consistent with the approach suggested by Cantwell[24,25] for characterizing the structure of time-dependent self-similar flows. This definition has also been suggested more recently by Vollmers[26] and Dallmann.[27] Since this definition depends only on the properties of the deformation tensor, it is independent of the frame of reference of the observer. Thus, whether or not a region of vorticity appears as a "vortex" depends on its environment, i.e., on the local rate-of-strain

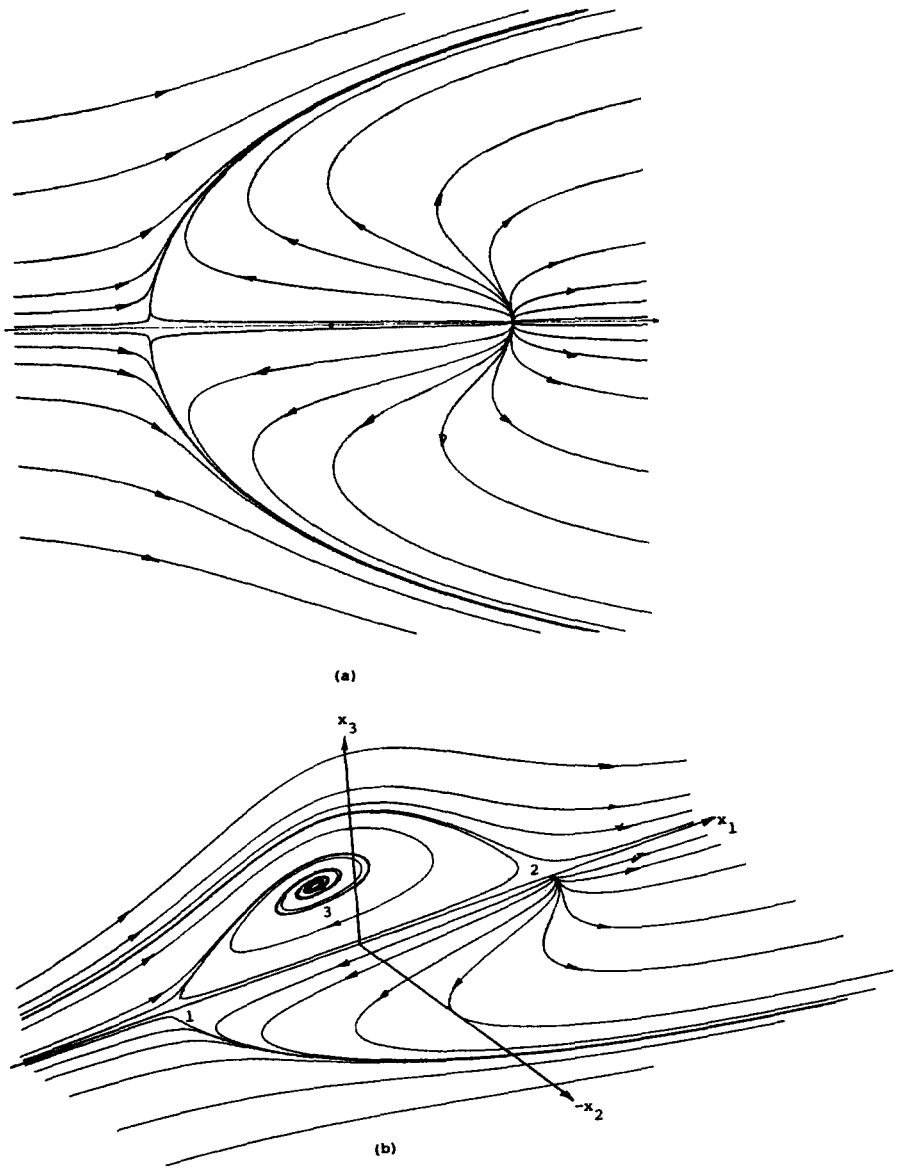

FIG. 6. Third-order symmetrical U separation. (a) Surface streamline pattern. (b) Oblique view showing the surface streamline pattern on the x_1-x_2 plane and solution trajectories in the plane of symmetry (i.e., x_1-x_3 plane).

field induced by motions outside of the region of interest.

A horseshoe vortex in isolation would have the properties of a vortex according to the velocity field definition discussed here. However, if it were to be placed in an environment of high rate of strain (which could be induced by surrounding horseshoe vortices), it may not appear as a vortex according to the velocity field definition. However, as far as the Biot–Savart law is concerned, it is no less a vortex than it would be if it were isolated. Thus in computations of the evolution of vortical flow fields it is the vorticity that is important and this quantity is independent of any nonrotating frame of reference. Vortices which conform with the velocity field definitions are of no special consequence, although they would possess special local mixing properties. Fluid interfaces tend to be rotated and wrapped when placed in such "vortices."

VII. SUMMARY OF *P-Q-R* SURFACES

The topological classification given in this paper maybe useful in the understanding of complicated flow patterns. The invariants P, Q, and R of a three-dimensional set of linear first-order differential equations define the topology of possible patterns. The boundaries between the different possible topological patterns are surfaces which are defined by the following equations.

(a) Surface S_1, i.e.,

$$27R^2 + (4P^3 - 18PQ)R + (4Q^3 - P^2Q^2) = 0.$$

This surface divides the region of the complex solutions from the region of real solutions. On this surface the eigenvalues are real but at least two of them are equal. All the eigenvalues are real and equal at the cusp.

(b) Surface S_2, i.e.,

$$PQ - R = 0.$$

This surface divides the complex region into two regions: one where the solution trajectories are unstable and one where the solution trajectories are stable. On this surface the complex eigenvalues are purely imaginary, the pattern is degenerate, and we obtain a center.

(c) Plane surface $R = 0$. On this surface the pattern is

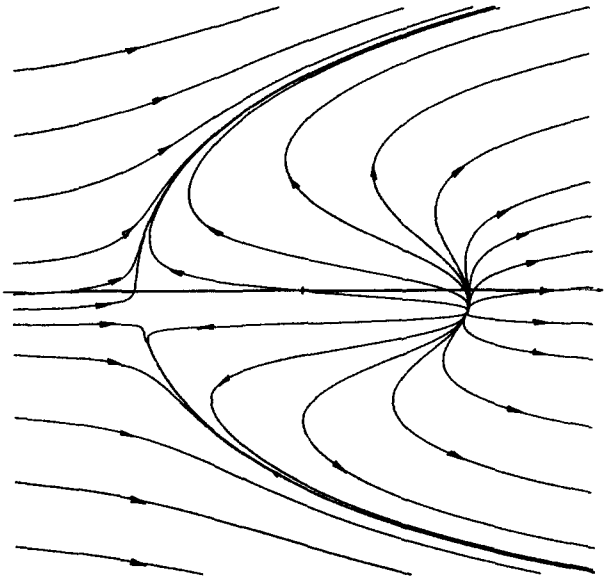

(a)

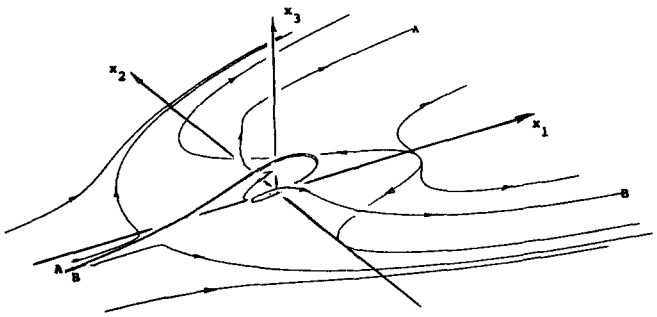

(b)

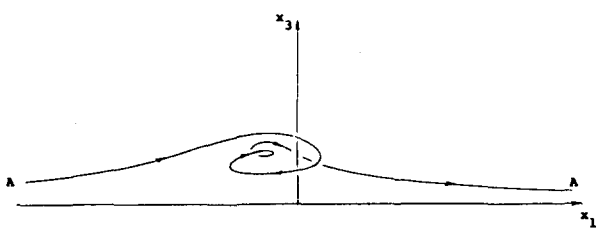

(c)

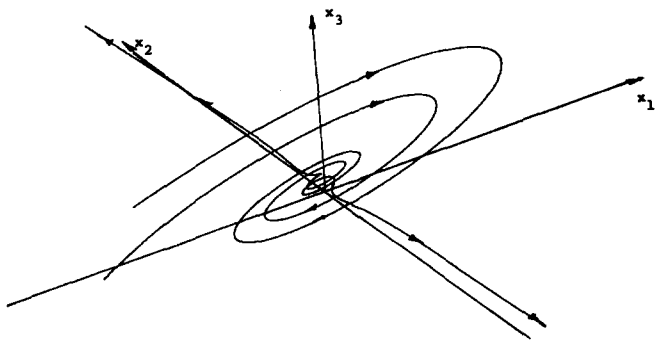

(d)

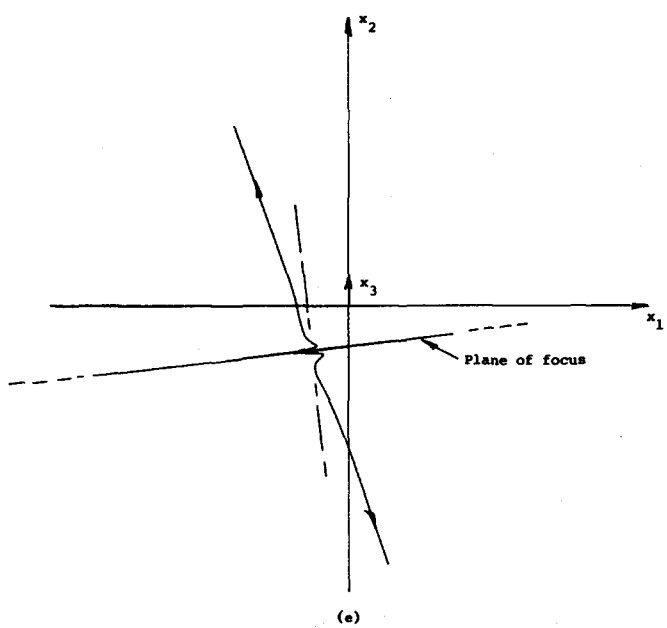

(e)

FIG. 7. Third-order unsymmetrical U separation. (a) Surface streamline pattern. (b) Oblique view showing the surface streamline pattern and streamlines above the surface. All streamlines except for *A-A* and *B-B* are surface streamlines. (c) Side view of (b) showing streamline *A-A*. (d) Solution trajectories of the linearized solution about a critical point above the surface. The critical point is a focus. (e) View of (e) such that the plane containing the focus is viewed "edge-on."

two dimensional in canonical form. In noncanonical form the two-dimensionality is skewed.

(d) Plane surface $P = 0$. All possible critical points of a three-dimensional solenoidal vector field can be described in this plane. The eigenvector plane patterns have one node and two saddles and it is not possible to have centers unless the flow is two dimensional.

(e) Surface S_3, i.e.,

$$PQ + 2P^3 + R = 0.$$

For incompressible fluids, all no-slip critical points must lie on this surface.

VIII. CONCLUSIONS

All possible linear local flow trajectories of a moving continuum for both compressible and incompressible fluids

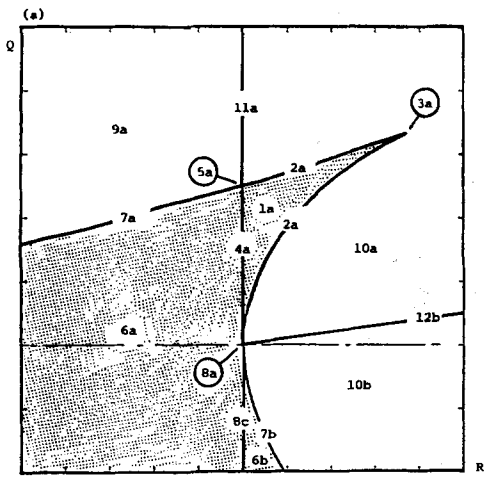

Q-R PLANE (P > 0)

1a. stable node/stable node/stable node
2a. stable node/stable node/stable star node
3a. stable star node/stable star node/stable star node
4a. stable line node-saddle/stable line node-saddle/stable node
5a. stable line node-saddle/stable line node-saddle/stable star node
6a. stable node/saddle/saddle
6b. unstable node/saddle/saddle
7a. stable star node/saddle/saddle
7b. unstable star node/saddle/saddle
8a. stable line node-saddle/stable line node-saddle/no flow
8c. stable line node-saddle/unstable line node-saddle/no flow
9a. stable focus/stretching (b >0)
10a. stable focus/compressing (b < 0)
10b. unstable focus/compressing (b < 0)
11a. stable focus/no flow (b = 0)
12b. center /compressing(b < 0)

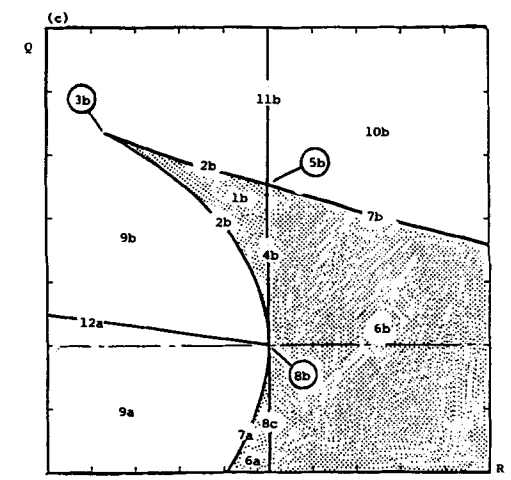

Q-R PLANE (P < 0)

1b. unstable node/unstable node/unstable node
2b. unstable node/unstable node/unstable star node
3b. unstable star node/unstable star node/unstable star node
4b. unstable line node-saddle/unstable line node-saddle/unstable node
5b. unstable line node-saddle/unstable line node-saddle/unstable star node
6a. stable node/saddle/saddle
6b. unstable node/saddle/saddle
7a. stable star node/saddle/saddle
7b. unstable star node/saddle/saddle
8b. unstable line node-saddle/unstable line node-saddle/no flow
8c. stable line node-saddle/unstable line node-saddle/no flow
9a. stable focus/stretching (b >0)
9b. unstable focus/stretching (b >0)
10b. unstable focus/compressing (b < 0)
11b. unstable focus/no flow (b = 0)
12a. center /stretching (b > 0)

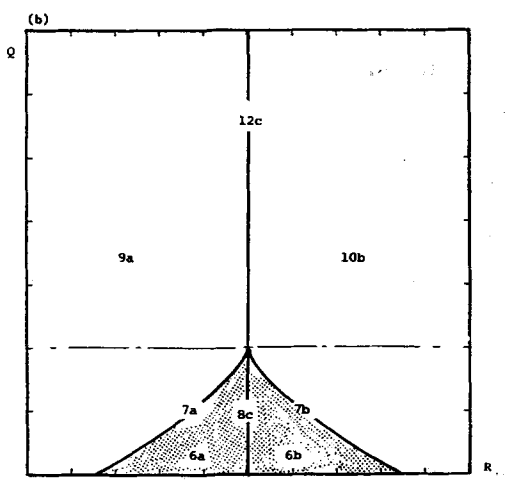

Q-R PLANE (P = 0)

6a. stable node/saddle/saddle
6b. unstable node/saddle/saddle
7a. stable star node/saddle/saddle
7b. unstable star node/saddle/saddle
8c. stable line node-saddle/unstable line node-saddle/no flow
9a. stable focus/stretching (b >0)
10b. unstable focus/compressing (b < 0)
12c. center /no flow(b = 0)

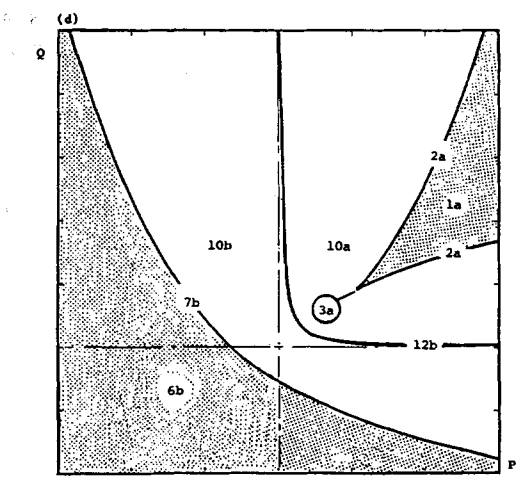

P-Q PLANE (R > 0)

1a. stable node/stable node/stable node
2a. stable node/stable node/stable star node
3a. stable star node/stable star node/stable star node
6b. unstable node/saddle/saddle
7b. unstable star node/saddle/saddle
10a. stable focus/compressing (b < 0)
10b. unstable focus/compressing (b < 0)
12b. center /compressing(b < 0)

FIG. 8. Classification of critical points in P-Q-R space. (a)–(c) Planes of constant P. (d)–(f) Planes of constant R.

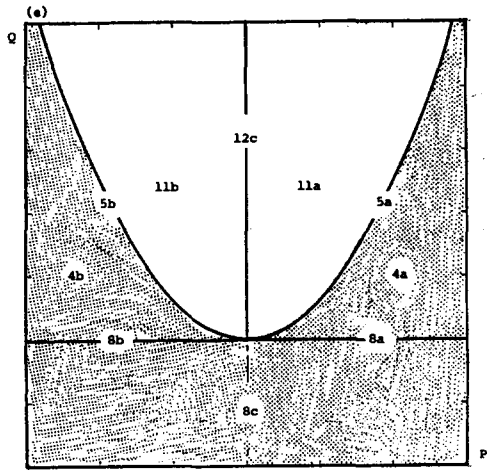

P-Q PLANE (R = 0)

4a. stable line node-saddle/stable line node-saddle/stable node
4b. unstable line node-saddle/unstable line node-saddle/unstable node
5a. stable line node-saddle/stable line node-saddle/stable star node
5b. unstable line node-saddle/unstable line node-saddle/unstable star node
8a. stable line node-saddle/stable line node-saddle/no flow
8b. unstable line node-saddle/unstable line node-saddle/no flow
8c. stable line node-saddle/unstable line node-saddle/no flow
11a. stable focus/no flow (b = 0)
11b. unstable focus/no flow (b = 0)
12c. center /no flow(b = 0)

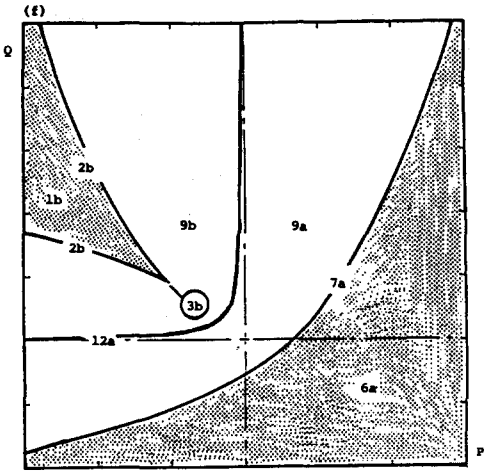

P-Q PLANE (R < 0)

1b. unstable node/unstable node/unstable node
2b. unstable node/unstable node/unstable star node
3b. unstable star node/unstable star node/unstable star node
6a. stable node/saddle/saddle
7a. stable star node/saddle/saddle
9a. stable focus/stretching (b >0)
9b. unstable focus/stretching (b >0)
12a. center /stretching (b > 0)

FIG. 8. (Continued).

can be completely categorized in the space of the rate-of-deformation tensor invariants P, Q, and R. A set of surfaces can be defined in this space which defines boundaries between topologically distinct flow patterns and serves as a guide for identifying critical points. Some useful properties of the P-Q-R space are illustrated and are applied to a frame invariant definition for a vortex, a skewed two-dimensional flow, and a three-dimensional separation pattern. Although the attention of this paper is focused on the velocity field and its associated rate-of-deformation tensor, the results are valid for any smooth three-dimensional vector field. For example, there may be situations where it is appropriate to work in terms of the vorticity field or pressure gradient field. In any case, it is expected that the results presented here will be of use in the interpretation of complex flow field data.

ACKNOWLEDGMENTS

Support from the Australian Research Council and U.S. Air Force Office of Scientific Research (AFOSR) Grant No. 84-0373D is gratefully acknowledged.

APPENDIX: CLASSIFICATION OF *P-Q-R* SPACE

All possible solution trajectories can be classified in the P-Q-R space. Figures 8(a)–8(c) show the location of the various three-dimensional critical points in constant P planes and Figs. 8(d)–8(f) show the locations in constant R planes. The possible types of three-dimensional critical points can be classified as follows.

1. Node/node/node

1a: Nodes are *stable* if

$$P>0, \quad 0<Q<P^2/3, \quad 0<R<R_b;$$

1b: nodes are *unstable* if

$$P<0, \quad 0<Q<P^2/3, \quad R_a<R<0$$

2. Node/node/star node

2a: Nodes are *stable* if

$$P>0, \quad P^2/4<Q<P^2/3, \quad R=R_a$$

or

$$P>0, \quad 0<Q<P^2/3, \quad R=R_b;$$

2b: nodes are *unstable* if

$$P<0, \quad P^2/4<Q<P^2/3, \quad R=R_a$$

or

$$P<0, \quad 0<Q<P^2/3, \quad R=R_b.$$

3. Star node/star node/star node

3a: Nodes are *stable* if

$$P>0, \quad Q=P^2/3, \quad R=R_a=R_b=P^3/27,$$

i.e., $R>0$;

3b: nodes are *unstable* if

$$P<0, \quad Q=P^2/3, \quad R=R_a=R_b=P^3/27,$$

i.e., $R<0$.

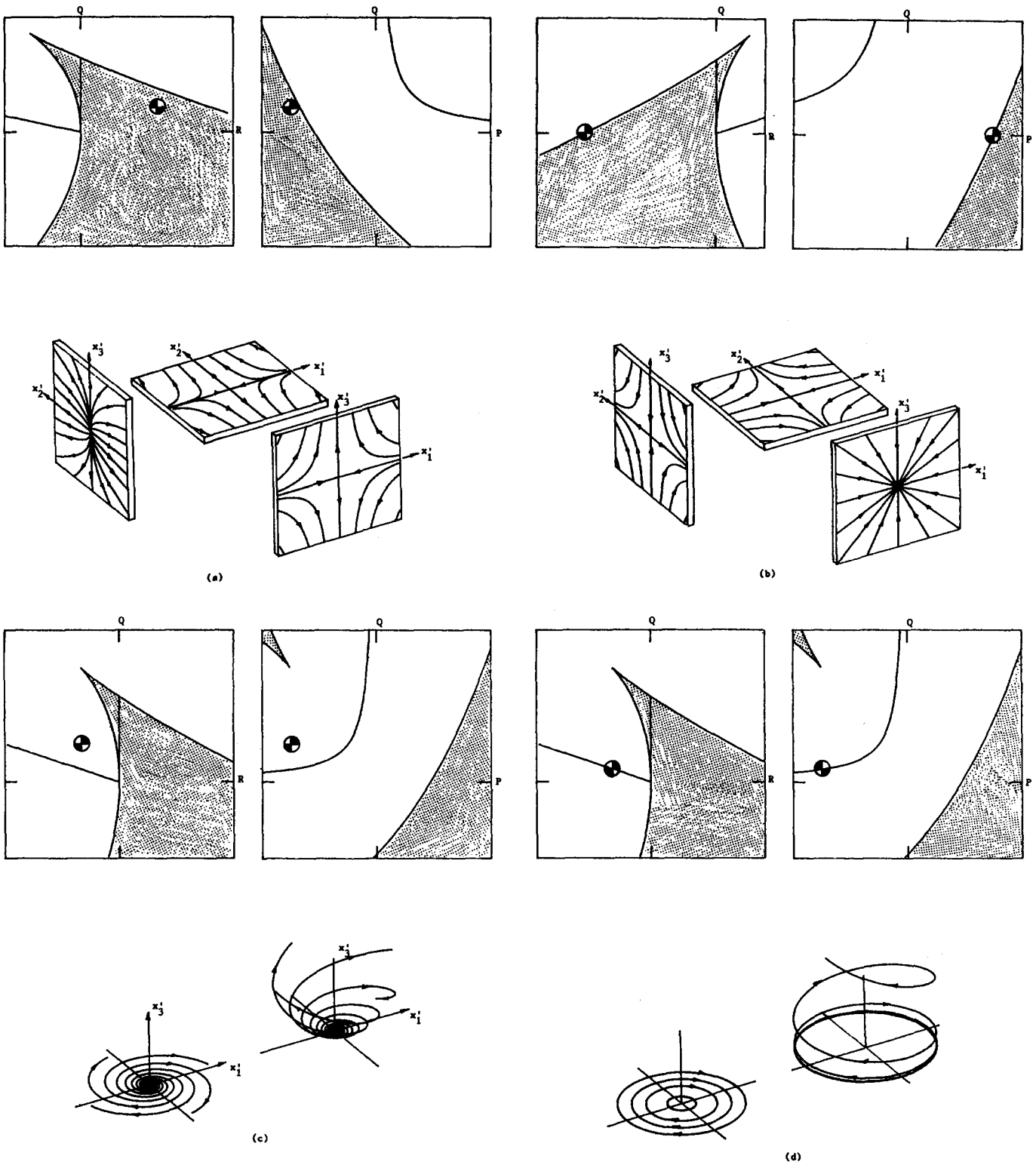

FIG. 9. Examples of three-dimensional critical points and their location in P-Q-R space (located by ◓). (a) Unstable node/saddle/saddle; (b) stable star node/saddle/saddle; (c) unstable focus/stretching ($b<0$); (d) center/stretching ($b>0$).

4. Line node–saddle/line node–saddle/node

4a: Nodes are *stable* if

$$P>0, \quad 0<Q<P^2/4, \quad R=0;$$

4b: nodes are *unstable* if

$$P<0, \quad 0<Q<P^2/4, \quad R=0.$$

5. Line node–saddle/line node–saddle/star node

5a: Nodes are *stable* if

$$P>0, \quad Q=P^2/4, \quad R=R_a=0;$$

5b: nodes are *unstable* if

$$P<0, \quad Q=P^2/4, \quad R=R_b=0.$$

6. Node/saddle/saddle

6a: Node is *stable* if

$$P \geqslant 0, \quad Q < P^2/4, \quad R_a < R < 0$$

or

$$P < 0, \quad Q < 0, \quad R_a < R < 0;$$

6b: node is *unstable* if

$$P \leqslant 0, \quad Q < P^2/4, \quad 0 < R < R_b$$

or

$$P > 0, \quad Q < 0, \quad 0 < R < R_b.$$

7. Star node/saddle/saddle

7a: Node is *stable* if

$$P \geqslant 0, \quad Q < P^2/4, \quad R = R_a \quad (\text{i.e., } R < 0)$$

or

$$P < 0, \quad Q < 0, \quad R = R_a \quad (\text{i.e., } R < 0);$$

note, when $P = 0$, $R = -(2\sqrt{3}/9)Q^{3/2}$.

7b: node is *unstable* if

$$P \leqslant 0, \quad Q < P^2/4, \quad R = R_b \quad (\text{i.e., } R > 0)$$

or

$$P > 0, \quad Q < 0, \quad R = R_b \quad (\text{i.e., } R > 0);$$

note, when $P = 0$, $R = +(2\sqrt{3}/9)Q^{3/2}$.

8. Line node–saddle/line node–saddle/no flow

8a: Both line node–saddles are *stable* if

$$P > 0, \quad Q = 0, \quad R = 0;$$

8b: both line node–saddles are *unstable* if

$$P < 0, \quad Q = 0, \quad R = 0;$$

8c: one line node–saddle is *stable* and the other is *unstable* if for all P,

$$Q < 0, \quad R = 0.$$

9. Focus/stretching ($b > 0$)

9a: Focus is *stable* if

$$P \geqslant 0, \quad Q > P^2/4, \quad R < 0,$$
$$P \geqslant 0, \quad Q < P^2/4, \quad R < R_a,$$
$$P < 0, \quad Q > 0, \quad R < PQ,$$
$$P < 0, \quad Q < 0, \quad R < R_a;$$

9b: focus is *unstable* if

$$P < 0, \quad Q > P^2/3, \quad PQ < R < 0,$$
$$P < 0, \quad P^2/4 < Q < P^2/3, \quad R_b < R < 0.$$
$$P < 0, \quad 0 < Q \leqslant P^2/3, \quad PQ < R < R_a.$$

10. Focusing/compressing ($b < 0$)

10a: Focus is *stable* if

$$P > 0, \quad Q > P^2/3, \quad 0 < R < PQ,$$
$$P > 0, \quad P^2/4 < Q < P^2/3, \quad 0 < R < R_a,$$
$$P > 0, \quad 0 < Q \leqslant P^2/3, \quad R_b < R < PQ;$$

10b: focus is *unstable* if

$$P \leqslant 0, \quad Q > P^2/4, \quad R > 0,$$
$$P \leqslant 0, \quad Q < P^2/4, \quad R > R_b,$$
$$P > 0, \quad Q > 0, \quad R < PQ,$$
$$P > 0, \quad Q < 0, \quad R > R_a.$$

11. Focus/no flow

11a: Focus is *stable* if

$$P > 0, \quad Q > P^2/4, \quad R = 0;$$

11b: focus is *unstable* if

$$P < 0, \quad Q > P^2/4, \quad R = 0.$$

12. Center

12a: *Stretching* ($b > 0$) if

$$P < 0, \quad Q > 0, \quad R = PQ;$$

12b: *compressing* ($b < 0$) if

$$P > 0, \quad Q > 0, \quad R = PQ;$$

12c: *no flow* ($b = 0$) if

$$P = 0, \quad Q > 0, \quad R = 0.$$

Note the association between the above listing of cases, the region identifiers in Figs. 8(a)–8(f), and the figure captions. The procedure for identifying the topology of a given flow is as follows.

(i) Locate the critical points of the vector field in question and evaluate various first partial derivatives at the points.

(ii) Evaluate P, Q, and R at the critical points. Locate these coordinates according to the above description of the boundaries of various domains. The topology of local solutions near each critical point is now known.

(iii) The time evolution of the flow topology is followed by repeating steps (i) and (ii) at each instant and plotting the resulting trajectories of each critical point in (P,Q,R) space. Bifurcations in the flow topology occur when critical points merge, split, or change type as their trajectories cross the boundaries between topological domains.

Some examples of the topology of the patterns in canonical form and their location in the P-Q-R space are given in Fig. 9.

[1] A. E. Perry and M. S. Chong, Annu. Rev. Fluid Mech. **19**, 125 (1987).
[2] U. Kaynak, T. L. Holst, B. J. Cantwell, and R. Sorenson, J. Aircr. **24**, 531 (1987).
[3] J. H. Chen, B. J. Cantwell, and N. N. Mansour, AIAA Paper No. 89-0285, 1989.
[4] G. S. Lewis, B. J. Cantwell, U. Vandsburger, and C. T. Bowman, in *The 22nd International Symposium on Combustion* (The Combustion Institute, Pittsburgh, 1988), pp. 515–522.
[5] A. Blaquire, *Nonlinear System Analysis* (Academic, New York, 1966).
[6] J. W. Reyn, Z. Angew. Math. Phys. **15**, 540 (1964).
[7] W. Kaplan, *Ordinary Differential Equations* (Addison-Wesley, Reading, MA, 1958).
[8] L. S. Pontryagin, *Ordinary Differential Equations* (Addison-Wesley, Reading, MA, 1962).
[9] A. A. Andronov, A. A. Vitt, and S. E. Khaikin, *Theory of Oscillators* (Pergamon, Oxford, 1966).
[10] N. Minorsky, *Nonlinear Oscillators* (Van Norstrand, Princeton, NJ, 1962).

[11]A. E. Perry and B. D. Fairlie, Adv. Geophys. **18B**, 299 (1974).
[12]M. W. Hirsch and S. Smale, *Differential Equations, Dynamical Systems, and Linear Algebra* (Academic, New York, 1974).
[13]J. Guckenheimer and P. Holmes, *Nonlinear Oscillations, Dynamical Systems, and Bifurcations of Vector Fields* (Springer, New York, 1983).
[14]S. Wiggins, *Global Bifurcations and Chaos* (Springer, New York, 1988).
[15]K. Oswatitsch, in *K. Oswatitsch: Contributions to the Development of Gasdynamics—Selected Papers Translated (to English) on the Occasion of K. Oswatitsch's 70th Birthday*, edited by W. Schneider and M. Platzer (Vieweg, Braunschweig, 1958), pp. 6–18.
[16]M. J. Lighthill, in *Laminar Boundary Layers*, edited by L. Rosenhead (Oxford, U.P., New York, 1963), pp. 48–88.
[17]A. E. Perry and H. G. Hornung, Z. Flugwiss. Weltraumforsch. **8**, 155 (1984).
[18]A. E. Perry and M. S. Chong, J. Fluid Mech. **173**, 207 (1986).
[19]H. J. Lugt, in *Recent Developments in Theoretical and Experimental Fluid Mechanics*, edited by U. Miller, K. G. Roesner, and B. Schmidt (Springer, Berlin, 1979), pp. 309–321.
[20]S. J. Kline, *Zorin Zaric Memorial International Seminar on Near-Wall Turbulence*, Dubrovnik, Yugoslavia, May 16–20 (Hemisphere, Washington, DC, 1988).
[21]P. R. Spalart, J. Fluid Mech. **187**, 61 (1988); *Ibid.*, NASA Tech. Memo. 89407 (1986).
[22]S. K. Robinson, S. J. Kline, and P. R. Spalart, in Ref. 20.
[23]B. J. Cantwell and G. A. Allen, Jr., in *Proceedings of the IUTAM Symposium on Turbulence and Chaotic Phenomena in Fluids*, edited by T. Tatsumi (North-Holland, Amsterdam, 1983), pp. 123–132.
[24]B. J. Cantwell, Arch. Mech. (Arch. Mech. Stosowanej) **31**, 707 (1978).
[25]B. J. Cantwell, J. Fluid Mech. **104**, 369 (1981).
[26]H. Vollmers, *AGARD Symposium on Aerodynamics of Vortical Type Flow in Three-Dimensions*, Rotterdam, 1983; AGARD-CP 342, 1983, pp. 14-1–14-14.
[27]U. Dallmann, DFVLR Report No. IB No. 221-82-A07, 1983.